




ARTICLE

# Genetic models reveal origin, persistence and non-redundant functions of IL-17-producing $\gamma\delta$ T cells

Inga Sandrock<sup>1</sup>, Annika Reinhardt<sup>1</sup>, Sarina Ravens<sup>1</sup>, Christoph Binz<sup>1</sup>, Anneke Wilharm<sup>1</sup>, Joana Martins<sup>1</sup>, Linda Oberdörfer<sup>1</sup>, Likai Tan<sup>1</sup>, Stefan Lienenklaus<sup>1,2</sup> , Baojun Zhang<sup>3</sup>, Ronald Naumann<sup>4</sup>, Yuan Zhuang<sup>3</sup>, Andreas Krueger<sup>1</sup> , Reinhold Förster<sup>1</sup>, and Immo Prinz<sup>1</sup> 

$\gamma\delta$  T cells are highly conserved in jawed vertebrates, suggesting an essential role in the immune system. However,  $\gamma\delta$  T cell-deficient *Tcrd*<sup>-/-</sup> mice display surprisingly mild phenotypes. We hypothesized that the lack of  $\gamma\delta$  T cells in constitutive *Tcrd*<sup>-/-</sup> mice is functionally compensated by other lymphocytes taking over genuine  $\gamma\delta$  T cell functions. To test this, we generated a knock-in model for diphtheria toxin-mediated conditional  $\gamma\delta$  T cell depletion. In contrast to IFN- $\gamma$ -producing  $\gamma\delta$  T cells, IL-17-producing  $\gamma\delta$  T cells (T $\gamma\delta$ 17 cells) recovered inefficiently after depletion, and their niches were filled by expanding Th17 cells and ILC3s. Complementary genetic fate mapping further demonstrated that T $\gamma\delta$ 17 cells are long-lived and persisting lymphocytes. Investigating the function of  $\gamma\delta$  T cells, conditional depletion but not constitutive deficiency protected from imiquimod-induced psoriasis. Together, we clarify that fetal thymus-derived T $\gamma\delta$ 17 cells are nonredundant local effector cells in IL-17-driven skin pathology.

## Introduction

$\gamma\delta$  T cells constitute one of three conserved lymphocyte populations rearranging clonal antigen receptors. Compared with  $\alpha\beta$  T cells and B cells,  $\gamma\delta$  T cells account for a smaller fraction of lymphocytes in blood and secondary lymphoid organs, but are more abundant in mucosal tissues and skin (Chien et al., 2014). There, IL-17-producing  $\gamma\delta$  T cells (T $\gamma\delta$ 17 cells) are thought to be the main source of the pro-inflammatory cytokines IL-17A and IL-17F, which protect the body's surfaces from fungal (Puel et al., 2011; Conti et al., 2014) and bacterial infections (Cho et al., 2010; Sumaria et al., 2011; Misiak et al., 2017) and play a role in the regulation of adipose tissue homeostasis and thermogenesis (Kohlgruber et al., 2018). But T $\gamma\delta$ 17 cells are also involved in the pathogenesis of inflammatory and autoimmune diseases (Papotto et al., 2017b, 2018), in particular experimental autoimmune encephalomyelitis (Petermann et al., 2010), spondyloarthritis (Reinhardt et al., 2016) and psoriasis (Cai et al., 2011; Pantelyushin et al., 2012; Ramírez-Valle et al., 2015). In mice, fetal V $\gamma$ 6<sup>+</sup> and a fraction of early V $\gamma$ 4<sup>+</sup> cells already differentiate in the prenatal thymus into T $\gamma\delta$ 17 effector cells and then egress to populate a wide range of organs (Jensen et al., 2008; Haas et al., 2009, 2012; Ribot et al., 2009). However, recent findings challenged the

view that all T $\gamma\delta$ 17 effector cells are exclusively derived from fetal thymus by showing that under certain circumstances, T $\gamma\delta$ 17 cells may also develop in adult mice, e.g., by recognition of cognate antigen (Zeng et al., 2012) or by TCR stimulation in the presence of IL-1 $\beta$  and IL-23 (Muschaweckh et al., 2017; Papotto et al., 2017a; Zarin et al., 2018).

In peripheral tissues, the large majority of T $\gamma\delta$ 17 cells display TCRs with rearrangements using V $\gamma$ 4 or V $\gamma$ 6 segments (Prinz et al., 2013). Many V $\gamma$ 4<sup>+</sup> and V $\gamma$ 6<sup>+</sup> T $\gamma\delta$ 17 cells show canonical semi-invariant TCR rearrangements without additions of non-templated N nucleotides (Kashani et al., 2015; Wei et al., 2015), supporting the hypothesis that their capacity to produce IL-17 cytokines is prewired in a subset of fetal T cell precursors before and independent of antigen-specific TCR selection (Haas et al., 2012; Prinz et al., 2013). In some tissues, particularly in the dermis, virtually all  $\gamma\delta$  T cells share a T $\gamma\delta$ 17 phenotype and are likely tissue-resident (Gray et al., 2011; Mabuchi et al., 2011; Sumaria et al., 2011; Jiang et al., 2017). Furthermore, it is still unclear to what extent the task of local IL-17 cytokine production is distributed between T $\gamma\delta$ 17 cells, Th17 cells, and IL-17-producing innate lymphoid cells (ILC3s) and whether these sources may actually be re-

<sup>1</sup>Institute of Immunology, Hannover Medical School, Hannover, Germany; <sup>2</sup>Institute for Laboratory Animal Science and Central Animal Facility, Hannover Medical School, Hannover, Germany; <sup>3</sup>Department of Immunology, Duke University Medical Center, Durham, NC; <sup>4</sup>Max-Planck-Institute of Molecular Cell Biology and Genetics, Dresden, Germany.

Correspondence to Immo Prinz: [prinz.immo@mh-hannover.de](mailto:prinz.immo@mh-hannover.de); A. Reinhardt's present address is Division of Immunology and Allergy, Department of Medicine, Solna, Karolinska Institutet, Stockholm, Sweden; B. Zhang's present address is Department of Pathogenic Microbiology and Immunology, School of Basic Medical Sciences, Xi'an Jiaotong University, Xi'an, Shaanxi, China; A. Krueger's present address is Institute of Molecular Medicine, Goethe University Frankfurt am Main, Frankfurt am Main, Germany.

© 2018 Sandrock et al. This article is distributed under the terms of an Attribution–Noncommercial–Share Alike–No Mirror Sites license for the first six months after the publication date (see <http://www.rupress.org/terms/>). After six months it is available under a Creative Commons License (Attribution–Noncommercial–Share Alike 4.0 International license, as described at <https://creativecommons.org/licenses/by-nc-sa/4.0/>).

dundant (Cua and Tato, 2010; Korn and Petermann, 2012; Sutton et al., 2012). To separate the specific physiological roles of  $\gamma\delta 17$  and other IL-17-producing cells, several studies used monoclonal antibodies that may lead to blocking and internalization of the  $\gamma\delta$  TCR, sometimes with significant biological effects (Rose et al., 1996; Pöllinger et al., 2011; Blink et al., 2014). However, we have previously shown that treatment with anti-TCR antibodies including the clones GL3 and UC7-13D5 does not deplete  $\gamma\delta$  T cells in vivo, but rather leads to TCR internalization and thereby generates “invisible”  $\gamma\delta$  T cells (Koenecke et al., 2009). Additionally, TCR delta chain knock-out mice (*Tcrd*<sup>-/-</sup>) are a very useful loss-of-function system for studying T cell development and  $\gamma\delta$  T cell function (Itoharu et al., 1993; Roberts et al., 1996; Welniak et al., 2001). However, the immune phenotype of *Tcrd*<sup>-/-</sup> mice is surprisingly mild (Mombaerts et al., 1993; Ramsburg et al., 2003), possibly because plastic  $\alpha\beta$  T cells can somehow occupy the niches of absent  $\gamma\delta$  T cells and might partially take over their functions (Jameson et al., 2004).

Here we investigated the regenerative capacity and function of  $\gamma\delta 17$  cells in vivo in immunocompetent mice. To this end, we generated a novel genetic knock-in model for diphtheria toxin (DTx)-mediated conditional  $\gamma\delta$  T cell depletion, and additionally used an inducible  $\gamma\delta$  T cell-specific Cre system to track the relative persistence of  $\gamma\delta$  T cell subsets in vivo. These genetic systems allowed us to revisit and compare the regenerative capacity between adult  $\gamma\delta 17$  cells and other  $\gamma\delta$  T cell subsets and to explore the function of  $\gamma\delta$  T cells in vivo.

## Results

To investigate the function of  $\gamma\delta$  T cells by conditional depletion in immunocompetent mice with normal  $\gamma\delta$  T cell compartments, we generated *Tcrd*-GDL mice expressing enhanced GFP (eGFP), human DTx receptor (DTR), and luciferase under the control of an IRES in the 3'UTR of the *Tcrd* constant gene (Fig. S1). The  $\gamma\delta$  T cell-specific cytoplasmic eGFP expression served to directly visualize  $\gamma\delta$  T cell morphology and their tissue-screening activity in skin and intestinal mucosa in vivo (Fig. 1, A and B; and Videos 1 and 2). Upon injection of luciferin substrate, luciferase activity indicated the distribution of  $\gamma\delta$  T cells across tissues (Fig. 1 C). Notably,  $\gamma\delta$  T cell-specific DTR expression enabled us to efficiently and truly deplete  $\gamma\delta$  T cells in homozygous *Tcrd*-GDL mice by a single DTx treatment without compromising peripheral CD4<sup>+</sup> and CD8<sup>+</sup>  $\alpha\beta$  T cells (Fig. 1 D and Fig. S2, A–C). Nevertheless, the DTR (along with eGFP and luciferase) is expressed in maturing thymocytes via germline promoters of the *Tcrd* constant gene before the *Tcrd* locus is excised during *Tcr* rearrangement at the CD4/CD8 double-positive stage (Fig. S2 D; Carabana et al., 2005; Prinz et al., 2006), and thus, thymic cellularity was transiently compromised after DTx treatment (Fig. S2 D). After conditional depletion,  $\gamma\delta$  T cells reappeared quickly already within 2 wk (Fig. 2 A), suggesting that the induced  $\gamma\delta$  T cell deficiency was partially reversible. However, distinct  $\gamma\delta$  T cell subsets showed divergent regeneration kinetics. CD27<sup>+</sup>CD44<sup>low</sup>  $\gamma\delta$  T cells with an IFN- $\gamma$ -producing phenotype fully regained predeletion levels in peripheral LNs (pLN) and spleen after 7 wk, while  $\gamma\delta 17$  cells, as defined by their CD27<sup>-</sup>CD44<sup>high</sup> phenotype, were poorly reconsti-

tuted (Fig. 2 B and Fig. S3 A). This finding is consistent with our previous data showing that  $\gamma\delta 17$  subsets do not develop de novo after bone marrow transplantation or after induction of T cell development in adult *Rag1*-deficient mice (Haas et al., 2012). Along this line, pLN V $\gamma$ 1<sup>+</sup> and intestinal V $\gamma$ 7<sup>+</sup> cells recovered efficiently (Fig. S3 B), but V $\gamma$ 6<sup>+</sup> and V $\gamma$ 4<sup>+</sup> cells did not (Fig. S3 C). Nevertheless, the rare  $\gamma\delta 17$  cells that were present at 8–9 wk after DTx treatment maintained a TCR repertoire that was similar to the TCR repertoire before depletion (Fig. 2 C), suggesting that these cells presumably originated from expansion of a few cells that survived the DTx treatment.

In skin, overall recovery of  $\gamma\delta$  T cells was very poor (Fig. 3 A). Nevertheless, via screening epidermal sheets, we could identify some V $\gamma$ 5<sup>+</sup> dendritic epidermal T cells (DETCs) that sporadically reappeared in isolated clonal patches (Fig. 3, B and C; and Video 3). Likely, a few individual DETCs resisted the DTx treatment, similar to the survival of some  $\gamma\delta 17$  cells described above. Of note, empty niches of conditionally depleted DETCs could not be invaded and repopulated by unconventional  $\alpha\beta$  T cells (Fig. S4). This is in contrast to the situation in constitutively  $\gamma\delta$  T cell-deficient *Tcrd*<sup>-/-</sup> mice, in which fetal-derived DETCs using  $\alpha\beta$  TCR populate the epidermis (Jameson et al., 2004). Interestingly, DTx treatment of heterozygous *Tcrd*<sup>GDL/WT</sup> mice induced a scattered “cow pattern” depletion of DETCs (Fig. 3 D). Together, these findings are consistent with the hypothesis that individual fetal DETC precursors colonize the epidermis early in life to form clonal lateral colonies (Payer et al., 1991).

To complement our results on the differential regeneration of  $\gamma\delta 17$  and other  $\gamma\delta$  T cell subsets with a fate mapping system, we next used an inducible  $\gamma\delta$  T cell-specific Cre system to track their relative persistence in vivo. Tamoxifen-induced Cre activation in *Tcrd*<sup>CreER</sup> × R26<sup>tdRFP</sup> mice (Zhang et al., 2015) led to permanent RFP gene expression in 33% of all  $\gamma\delta$  T cells in pLN and spleen and 20% in liver after 2 wk (Fig. 4, A and B). 7 wk after tamoxifen gavage, most CD27<sup>+</sup>CD44<sup>low</sup>  $\gamma\delta$  T cells with an IFN- $\gamma$ -producing phenotype had lost their RFP label, suggesting that this subset is constantly replenished by newly generated  $\gamma\delta$  T cells from the thymus (Fig. 4 C). At the same time, the frequency of RFP-labeled cells among CD27<sup>-</sup>CD44<sup>high</sup>  $\gamma\delta 17$  cells was highly persistent in pLN, spleen, and liver after 7 wk (Fig. 4 C). In the skin of *Tcrd*<sup>CreER</sup> × R26<sup>tdRFP</sup> mice, genetic labeling of both epidermal and dermal  $\gamma\delta$  T cells was remarkably efficient (Fig. 4 D). However, the frequency of dermal RFP<sup>+</sup>  $\gamma\delta$  T cells but not of epidermal RFP<sup>+</sup> DETCs decreased after 7 wk, indicating a higher turnover of  $\gamma\delta 17$  cells infiltrating the dermis as compared with  $\gamma\delta 17$  cells in pLN. It is thus conceivable that dermal  $\gamma\delta 17$  cells may also exchange with distant tissues including lymph nodes (Hartwig et al., 2015; Ramírez-Valle et al., 2015), in line with the idea that effector  $\gamma\delta$  T cells with a  $\gamma\delta 17$  phenotype can be selectively trapped in lymph nodes (Chennupati et al., 2010; Romagnoli et al., 2016; Audemard-Verger et al., 2017; Ugur et al., 2018).

Next, we investigated the impact of  $\gamma\delta$  T cell depletion in *Tcrd*-GDL mice in imiquimod (IMQ)-induced skin pathology (van der Fits et al., 2009; Cai et al., 2011; Pantelyushin et al., 2012). We hypothesized that  $\gamma\delta 17$  cells should play crucial and nonredundant roles in this experimental model for human psoriasis, because the importance of  $\gamma\delta 17$  cells inducing psoriasis pathology was

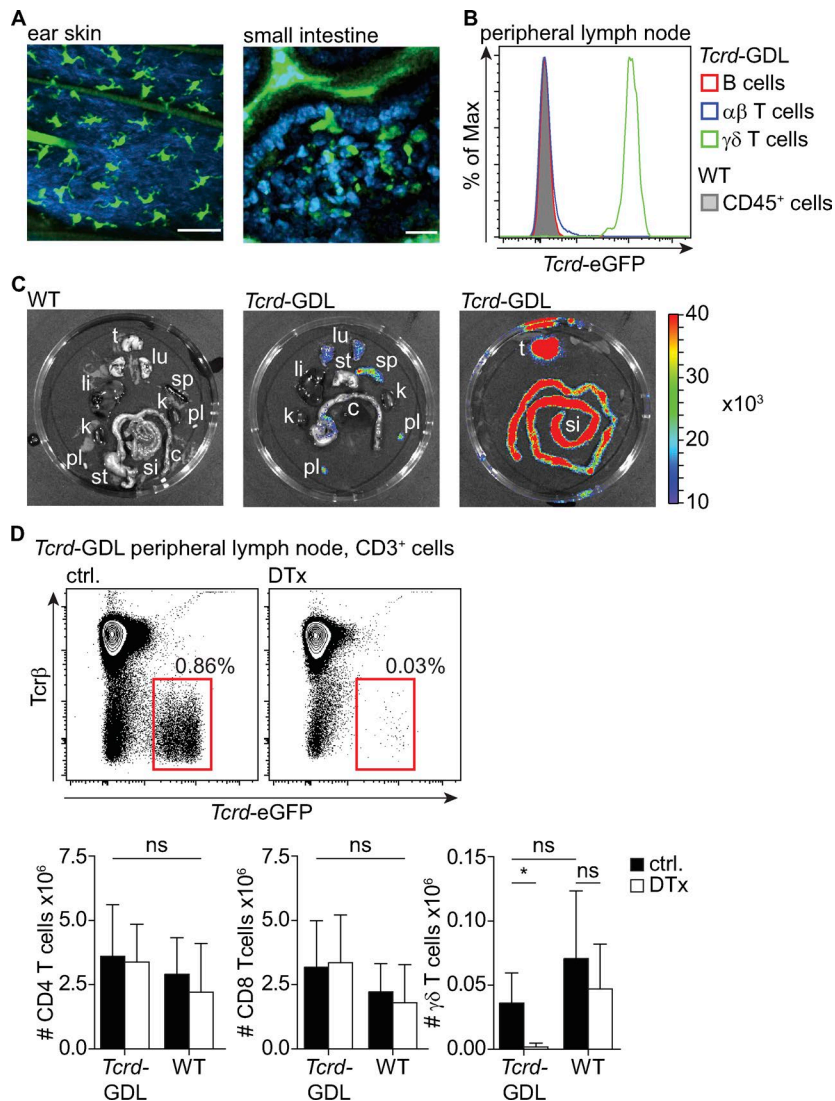


**Figure 1. eGFP, luciferase, and DTx receptor are functionally expressed by  $\gamma\delta$  T cells.** (A) Two-photon in vivo imaging of *Tcrd*-GDL mouse ear skin and small intestine. Green,  $\gamma\delta$  T cell eGFP; blue, second harmonics (ear skin) or Hoechst 33342 nuclear staining (small intestine). Bars: 50  $\mu$ m (ear skin); 15  $\mu$ m (small intestine; see also Videos 1 and 2). (B) eGFP expression by peripheral lymph node  $\gamma\delta$  T cells (green, gated as CD45<sup>+</sup>Tcr $\beta$ <sup>+</sup>CD3<sup>+</sup>TCR $\gamma\delta$ <sup>+</sup>),  $\alpha\beta$  T cells (blue, gated as CD45<sup>+</sup>Tcr $\beta$ <sup>+</sup>CD3<sup>+</sup>), and B cells (red, gated as CD45<sup>+</sup>Tcr $\beta$ <sup>+</sup>CD3<sup>+</sup>CD19<sup>+</sup>) of a *Tcrd*-GDL mouse and CD45<sup>+</sup> cells of a C57BL/6-NCrl mouse (WT, filled gray line). Shown is one representative histogram of two experiments with each  $n = 2$ –3 mice per group. (C) Bioluminescence by functional luciferase expression was detected by IVIS in at least two independent experiments with  $n = 1$ –2 mice each. C57BL/6-NCrl WT and *Tcrd*-GDL were sacrificed 10 min after injection of D-luciferin and the indicated organs were displayed for imaging. Color bar corresponds to signal intensities measured as photons. c, colon; k, kidney; li, liver; lu, lung; pl, peripheral lymph node; si, small intestine; sp, spleen; st, stomach; t, thymus. (D) Depletion of  $\gamma\delta$  T cells using DTx was analyzed by flow cytometry. Representative contour plot of pLN T cells (CD3<sup>+</sup> cells) of *Tcrd*-GDL mice treated with PBS (ctrl.) or DTx (top). Cell counts of indicated cell populations in pLNs of DTx- (white bars) and PBS- (black bars) injected *Tcrd*-GDL and C57BL/6-NCrl WT mice (bottom). Bar graphs show pooled data from four independent experiments with each  $n = 1$ –3 mice per group, Kruskal Wallis test with Dunn's Multiple Comparison post-tests. \*,  $P < 0.05$ ; ns, not significant.

suggested before in this IMQ model (Cai et al., 2011; Pantelyushin et al., 2012), as well as in a related model for psoriasis based on intradermal IL-23 injection (Mabuchi et al., 2011, 2013) and in the human system (Laggner et al., 2011). However, constitutively  $\gamma\delta$  T cell-deficient *Tcrd*<sup>-/-</sup> mice showed similar neutrophil influx (Fig. 5 A), disease scores, and epidermal thickening as compared with  $\gamma\delta$  T cell-sufficient mice after IMQ treatment (Fig. 5, B and C). In contrast, these disease parameters were significantly reduced in acutely depleted *Tcrd*-GDL mice (Fig. 5, A–C), likely because the absence of pathogenic T $\gamma\delta$ 17 cells led to an overall decrease of IL-17-producing dermal lymphocytes (Fig. 5 D). Thus, acute depletion of  $\gamma\delta$  T cells in *Tcrd*-GDL mice, but not constitutive absence of  $\gamma\delta$  T cells in *Tcrd*<sup>-/-</sup> mice, conferred a strong protection against psoriasis pathology. Additionally, direct visualization of motile dermal  $\gamma\delta$  T cells that migrated across the basement membrane straight into the inflamed epidermis of IMQ-treated skin further supported a direct and tissue-confined contribution of  $\gamma\delta$  T cells to epidermal inflammation in IMQ-induced psoriasis (Fig. 6, A–C; and Video 4). However, analysis of the track straightness and mean track speed of the motile  $\gamma\delta$  T cells entering the inflamed epidermal layers was not altered, refuting the hypoth-

esis that their movement was driven by antigen-specific cell-to-cell interactions with epidermal cells (Fig. 6 B).

Next, we investigated the regeneration of dermal IL-17 immunity after conditional depletion of  $\gamma\delta$  T cells. Despite the sustained lack of T $\gamma\delta$ 17 cells in the dermis of DTx-treated *Tcrd*-GDL mice (Fig. 3 A), overall frequencies of IL-17-producing dermal CD45<sup>+</sup> lymphocytes rebounded to pretreatment levels within 2 mo, in part through expansion of a few surviving T $\gamma\delta$ 17 cells, but mainly due to an increased abundance of TCRThy1<sup>+</sup> ILC3s (Fig. 7 A). While T $\gamma\delta$ 17 cells are the major population of IL23R<sup>+</sup> lymphocytes in the skin, Fig. 7 B shows that also some dermal ILCs and Th17 cells are expressing the IL-23R in steady state, and it is thus tempting to speculate that these are the cells that expand via elevated availability of homeostatic cytokines such as IL-23 in the absence of T $\gamma\delta$ 17 cells. Accordingly, previously depleted *Tcrd*-GDL mice regained susceptibility to IMQ-induced pathology (Fig. 7 C). Of note, the experiments shown in Fig. 7 C suggested that ear thickening in previously depleted and recovered *Tcrd*-GDL mice might still be less pronounced than in undepleted *Tcrd*-GDL mice or in *Tcrd*<sup>-/-</sup> mice, but the differences were marginal and based on statistical outliers. At 9 wk after de-



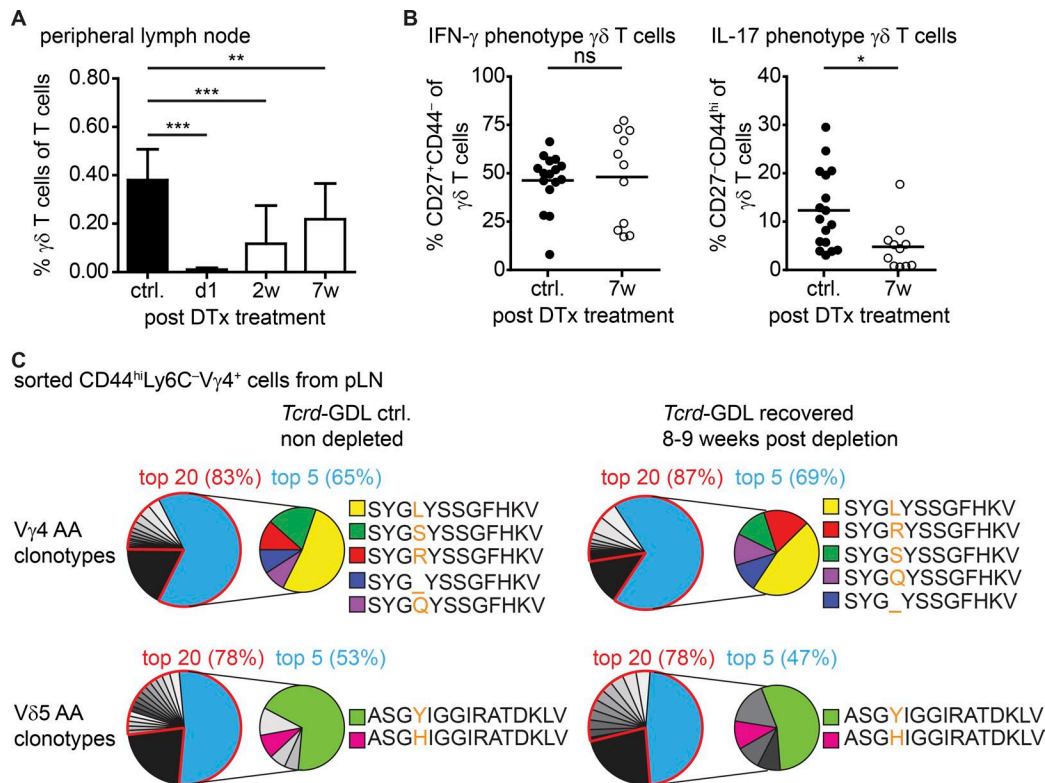


**Figure 2. Depletion of T $\gamma\delta$ 17 cells does not change their repertoire. (A and B)** Flow cytometric analysis of indicated cell populations 1 d (d1), 2 wk (2w), and 7 wk (7w) after depletion of  $\gamma\delta$  T cells in *Tcrd*-GDL littermate mice. Shown are pooled data from three independent experiments with each  $n = 2 - 5$  mice per group, Student's *t* test. **(A)** Bar graph shows frequencies of  $\gamma\delta$  T cells (Tcr $\beta$ <sup>+</sup>GFP<sup>+</sup>) among T cells (A.dead<sup>+</sup>CD3<sup>+</sup>) in peripheral lymph nodes, mean  $\pm$  SD. **(B)** Scatter plots show frequencies of indicated  $\gamma\delta$  T cell populations among all  $\gamma\delta$  T cells in peripheral lymph nodes, one dot represents one mouse, mean. **(C)** T cell receptor repertoire analysis of  $\gamma\delta$  T cell nondepleted (ctrl., left) and depleted *Tcrd*-GDL mice 8–9 wk after depletion (right). Sorted CD44<sup>hi</sup>Ly6C<sup>-</sup>V $\gamma$ 4<sup>+</sup> peripheral lymph node cells were pooled from 7–8 mice each and facilitated to Illumina NGS. Amplicons were generated by multiplex PCR. Proportions of V $\gamma$ 4 (top) and V $\delta$ 5 (bottom) top 20 and top 5 amino acid (AA) clonotypes among complete V $\gamma$ 4 and V $\delta$ 5 repertoires. Amino acid sequences of the top 5 clonotypes. \*,  $P < 0.05$ ; \*\*,  $P < 0.01$ ; \*\*\*,  $P < 0.001$ ; ns, not significant.

pletion and induction of psoriasis, IL-17 in cervical lymph nodes, including ear skin draining lymph nodes, was mainly produced by Th17  $\alpha\beta$  T cells and lineage-negative ILC3s (Th17,  $33.15 \pm 3.15\%$ ; ILC,  $48.97 \pm 6.37\%$ ; Fig. 7 D). This is in agreement with the hypothesis that pathogenic ILC3s in the skin of constitutively  $\gamma\delta$  T cell-deficient *Tcrd*<sup>-/-</sup> mice can compensate for the lack of  $\gamma\delta$  T cells (Pantelyushin et al., 2012; Gladiator et al., 2013). After depletion of T $\gamma\delta$ 17 cells in adult *Tcrd*-GDL mice, compensating ILC3s might have been recruited from the circulation; however, their established strict tissue-residency would advocate for local homeostatic expansion (Gasteiger et al., 2015). Nevertheless, the observed loss of protection at 9 wk after  $\gamma\delta$  T cell depletion could also be compensated in part due to the reappearance of T $\gamma\delta$ 17 cells in skin and pLN. To test this, we performed a second round of DTx treatment at 9 wk after a first ablation of  $\gamma\delta$  T cells (Fig. 8 A). This additional depletion regimen could efficiently reablate  $\gamma\delta$  T cells including the few recovered T $\gamma\delta$ 17 cells (Fig. 8 B), and as a consequence, the severity of IMQ-induced psoriasis as measured by ear thickening and disease score were again diminished after a second  $\gamma\delta$  T cell depletion (Fig. 8 C). Together, these data strongly suggest a nonredundant contribution of  $\gamma\delta$  T cells to epidermal inflammation in IMQ-induced psoriasis. Such an essential role of T $\gamma\delta$ 17 cells for psoriasis pathology was somehow expected from

previous observations in WT mice, but so far, experimental evidence was cloaked by compensatory expansion of other IL-17-producing lymphocytes in constitutively  $\gamma\delta$  T cell-deficient *Tcrd*<sup>-/-</sup> mice and became only clear after conditional ablation of  $\gamma\delta$  T cells in immunocompetent mice.

## Discussion

This work used  $\gamma\delta$  T cell-specific genetic systems to demonstrate that T $\gamma\delta$ 17 cells play nonredundant roles in IMQ-induced skin inflammation and clarified that they are poorly generated de novo in adult mice. Namely, we used tamoxifen-induced Cre activation in *Tcrd*<sup>CreER</sup>  $\times$  R26<sup>tdRFP</sup> mice (Zhang et al., 2015) to track the persistence of T $\gamma\delta$ 17 cells, and we established *Tcrd*-GDL mice for conditional depletion of  $\gamma\delta$  T cells mice that displayed an otherwise normal WT  $\gamma\delta$  T cell compartment. We expect that the *Tcrd*-GDL system will be instructive for delineating the physiological role of  $\gamma\delta$  T cells in a plethora of further experimental models for human disease.

Technically, injection of a relatively small dose of DTx was sufficient for depleting >96% of all  $\gamma\delta$  T cells. Of note, this procedure did not facilitate opportunistic infections, at least under specific pathogen-free conditions, nor did the treated mice suf-

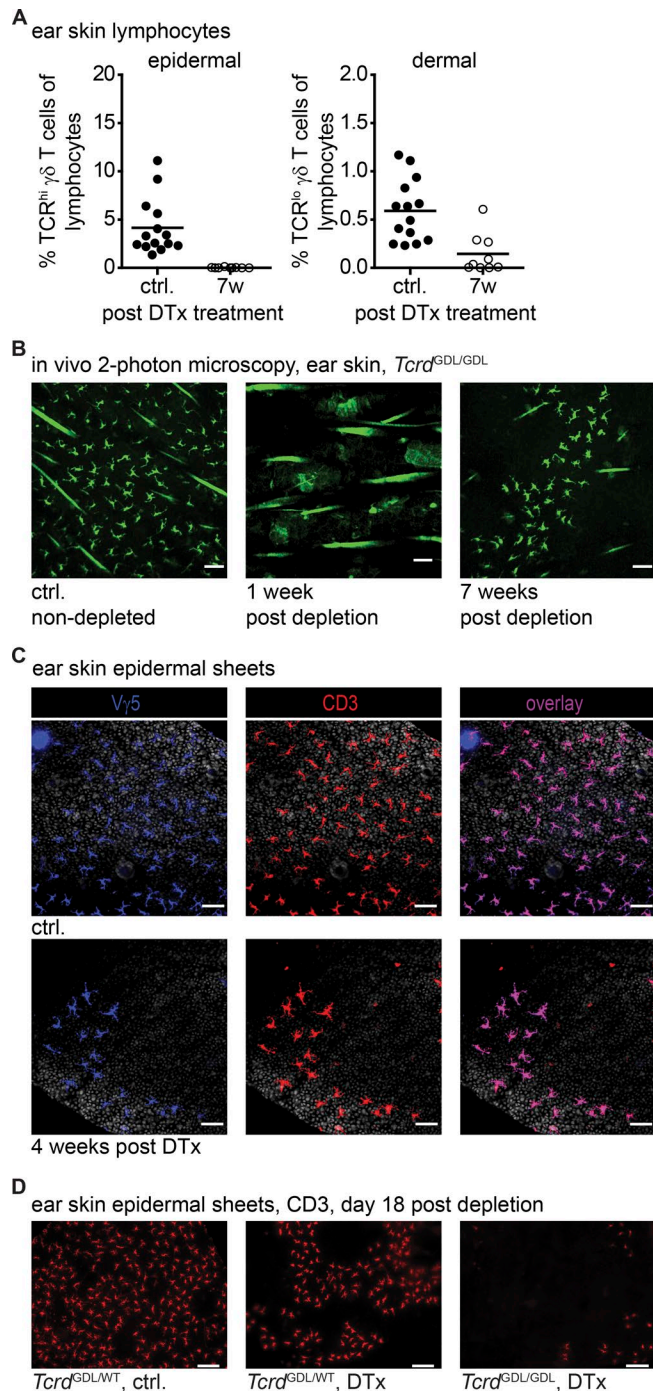


**Figure 3. Patchy depletion and recovery of ear skin  $\gamma\delta$  T cells.** (A) Frequencies of  $\gamma\delta$ TCR<sup>hi</sup> epidermal (left) and  $\gamma\delta$ TCR<sup>lo</sup> dermal (right)  $\gamma\delta$  T cells in nondepleted (ctrl.) and 7-wk-ago-depleted (7w) *Tcrd*-GDL mice. Pooled data from two independent experiments, one dot represents one mouse, mean. (B) Longitudinal in vivo two-photon imaging of *Tcrd*-GDL ear skin. Images were acquired from the same mouse at indicated time points after  $\gamma\delta$  T cell depletion. As reference, a mouse was injected with PBS (ctrl.). Green:  $\gamma\delta$  T cell eGFP by *Tcrd*-GDL mice, shown are representative images of two independent experiments. Bars, 50  $\mu$ m (see Video 3). (C) Epidermal sheets of DTx- and PBS (ctrl.)-treated *Tcrd*-GDL mice 4 wk after  $\gamma\delta$  T cell depletion. Representative fluorescence microscopy images out of two independent experiments with  $n = 1$ –2 mice each; blue: V $\gamma$ 5; red: CD3; white: DAPI nuclear staining. Bars, 50  $\mu$ m. (D) Epidermal sheets of hetero- and homozygous *Tcrd*-GDL mice were stained with anti-CD3 $\epsilon$  (red) 18 d after depletion (DTx) or PBS injection (ctrl.). Bars, 100  $\mu$ m. Staining was validated in three experiments with  $n = 1$ –2 mice each.

fer from intolerable barrier defects. Therefore, the system can be applied to investigate specific functions of  $\gamma\delta$  T cells in vivo. Furthermore, multiple rounds of quantitative  $\gamma\delta$  T cell depletion are possible because the DTR gene in the *Tcrd*-GDL strain is a knock-in to the 3'-UTR of the functional endogenous *Tcrd* constant gene and thus, depletion does not foster the outgrowth of DTR-negative  $\gamma\delta$  T cells as observed in BAC-transgenic systems (Lahl and Sparwasser, 2011). While peripheral  $\alpha\beta$  T cell populations were not significantly affected by DTx treatment of *Tcrd*-GDL mice, a limitation of the system is the observed collateral transient depletion of developing CD4/CD8 double-negative and double-positive  $\alpha\beta$  T cell precursors. This precludes using the model for direct assessment of  $\gamma\delta$  T cell functions within the thymus. On the other hand, this feature might serve to further revisit the kinetics of thymic  $\alpha\beta$  T cell development (McCaughy et al., 2007; Föhse et al., 2013).

Next to genetic ablation by immune cell-specific DTR expression (Walzer et al., 2007; Lahl and Sparwasser, 2011; van Blijswijk et al., 2013), monoclonal antibody (mAb)-mediated depletion via complement lysis is frequently used in loss-of-function studies without the need for breeding mutant mice. For example, NK cells in NK1.1-bearing mouse strains can be efficiently depleted by injection of the PK136 mAb (Koo and Peppard, 1984). However, in vivo ablation of  $\gamma\delta$  T cells using any currently available mAb does not work. As it had been suspected already for a long time (Kaufmann et al., 1993; Ke et al., 1997), *Tcrd*-H2BeGFP reporter mice could prove that injection of mAbs directed against the  $\gamma\delta$  TCR, such as clones UC7-13D5 (Houlden et al., 1989) or GL3 (Goodman and Lefrançois, 1989), does not deplete  $\gamma\delta$  T cells, but leads to TCR internalization and thereby generates “invisible”  $\gamma\delta$  T cells (Koenecke et al., 2009). Still, several studies found opposing effects of  $\gamma\delta$  T-cell depletion and adoptive transfer of  $\gamma\delta$  T cells, as well as similar experimental outcomes in *Tcrd*<sup>-/-</sup> and anti- $\gamma\delta$  TCR-treated mice. Therefore, mAb-mediated in vivo blocking of the  $\gamma\delta$  TCR could be seen as a “functional depletion” and as such is certainly useful to investigate the specific role of the  $\gamma\delta$  TCR in immune responses of  $\gamma\delta$  T cells, for example in response to malaria infection (Mamedov et al., 2018). Of note, the low efficiency of the  $\gamma\delta$  T cell-specific Cre system in *Tcrd*<sup>CreER</sup> mice (Zhang et al., 2015) precludes quantitative depletion of  $\gamma\delta$  T cells in ROSA-DTA mice (Voehringer et al., 2008).

Functionally, acute depletion of  $\gamma\delta$  T cells showed a different phenotype in IMQ-induced psoriasis as compared with constitutively deficient *Tcrd*<sup>-/-</sup> mice (Itoharu et al., 1993), i.e., protection versus susceptibility, respectively. This underlines previous findings that  $\alpha\beta$  T cells can invade the niches of absent  $\gamma\delta$  T cells and might partially take over their functions (Jameson et al., 2004). While compensatory  $\alpha\beta$  DETCs were not able to properly respond to keratinocyte damage like genuine  $\gamma\delta$  DETCs (Jameson et al., 2004), we show here that dermal ILC3 and Th17 cells were sufficient to induce psoriasis pathology in the absence of  $\gamma\delta$  T cells. An alternative explanation for protection of acutely depleted *Tcrd*-GDL mice from IMQ-induced psoriasis would be a strong imbalance of quickly regenerated V $\gamma$ 1 T cells and poorly regenerated IL-17-producing V $\gamma$ 4 and V $\gamma$ 6  $\gamma\delta$  T cells, which may subsequently alter the balance of other adaptive immune cells including  $\alpha\beta$  T cells and B cells (Huang et al., 2015, 2016). However, this inter-



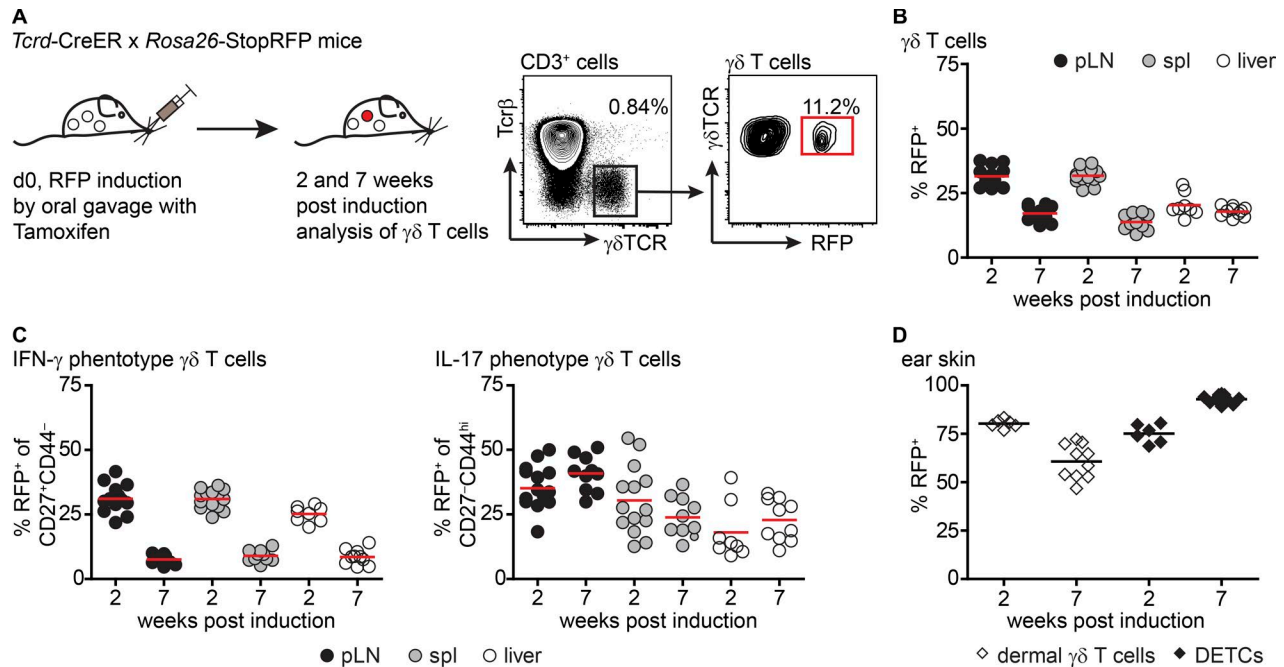


**Figure 4. Ty $\delta$ 17 cells are long lived and self-renewing.** (A) Inducible  $\gamma\delta$  T cell fate-mapping model. RFP expression in  $\gamma\delta$  T cells was induced by oral administration of tamoxifen (left). Representative gating for RFP<sup>+</sup> peripheral lymph node  $\gamma\delta$  T cells 7 wk after tamoxifen administration (right). (B and C) Analysis of RFP<sup>+</sup> cells from indicated tissues and time points after RFP induction. One dot equals one mouse, pooled data from three independent experiments with each three to six littermate mice per time point, mean. (B) Frequencies of RFP<sup>+</sup>  $\gamma\delta$  T cells. (C) Frequencies of RFP<sup>+</sup> cells among IFN- $\gamma$  (left) or IL-17 (right) phenotype  $\gamma\delta$  T cell subsets, defined as CD3<sup>+</sup>Tcr $\beta$ <sup>+</sup> $\gamma\delta$ TCR<sup>+</sup>CD44<sup>hi</sup>CD27<sup>+</sup> and CD3<sup>+</sup>Tcr $\beta$ <sup>+</sup> $\gamma\delta$ TCR<sup>+</sup>CD44<sup>hi</sup>CD27<sup>+</sup>, respectively. (D) Mean frequency of RFP<sup>+</sup> cells among skin-derived  $\gamma\delta$ TCR<sup>hi</sup> DETCs and  $\gamma\delta$ TCR<sup>lo</sup> dermal  $\gamma\delta$  T cells. One dot equals one mouse, pooled data from two experiments with each three to five littermate mice per time point, mean.

pretation is flawed by the finding that this imbalanced ratio of overrepresented V $\gamma$ 1 versus underrepresented (IL-17-producing) V $\gamma$ 4/6  $\gamma\delta$  T cells was still observed after 7 wk, a time point at which the previously depleted mice were no longer resistant to IMQ-induced psoriasis.

In any case, our observations may seem to be contrasting previous results that found significantly decreased IMQ-induced skin pathology in *Tcrd*<sup>-/-</sup> mice (Cai et al., 2011; Pantelyushin et al., 2012). However, experimental details such as the investigation of either IMQ-treated ear skin or back skin, along with the precise genetic background of the mice, and different microbiota might strongly bias the outcome of such experiments. Most importantly, skin microbiota can autonomously control the local inflammatory milieu and tune resident Th17 and CD8<sup>+</sup> T cell function (Naik et al., 2015; Muschawekkh et al., 2016). Even so, our study further underlines that Ty $\delta$ 17 cells are the major population of IL23R<sup>+</sup> lymphocytes in the skin and the main source of IL-17 in IMQ-induced inflammatory pathology in immunocompetent mice. The fact that this function can be compensated by other IL-17-producing lymphocytes in *Tcrd*<sup>-/-</sup> or *Rag*<sup>-/-</sup> mice highlights the biological importance of the IL-23-IL-17 cytokine axis for skin homeostasis and antimicrobial immunity (Gladiator et al., 2013; Conti et al., 2014). Also, in contrast to the mouse model, recent investigations of human psoriasis suggested that Ty $\delta$ 17 cells are rare in human psoriatic skin and rather outnumbered by Th17 cells with an innately biased TCR repertoire (Matos et al., 2017; Merleev et al., 2018). Furthermore, CD8<sup>+</sup> T cells have been implicated in the pathogenesis of human psoriasis (Hammar et al.,

1984; Di Meglio et al., 2016). A recent study showed that the CD8<sup>+</sup> T cell response in psoriasiform inflammation is controlled by regulatory T cells, as their depletion led to CD8<sup>+</sup> T cell expansion and exacerbated skin inflammation (Stockenhuber et al., 2018). At the same time, dermal  $\gamma\delta$  T cell expansion was not observed in regulatory T cell-depleted mice (Stockenhuber et al., 2018). This indicated that the IMQ-induced pathology after regulatory T cell depletion is driven by alternative pathways, possibly more resembling to human psoriasis pathology.

In future studies, the combination of *Tcrd*-GDL mice, *Tcrd*<sup>-/-</sup> mice, and  $\gamma\delta$  TCR blocking with mAbs will make a powerful triad of three independent loss-of- $\gamma\delta$  T cell-function strategies. Comparing their different phenotypes should be very helpful to elucidate the in vivo functions of  $\gamma\delta$  T cells in models for human disease including infections, autoimmunity, and cancer.

## Materials and methods

### Animals

*Tcrd*-GDL, *Tcrd*<sup>-/-</sup> (B6.129P2-Tcrdtm1Mom/J; Itohara et al., 1993), *Tcrd*CreERSx*Rosa26*-StopRFP mice, obtained by crossing *Tcrd*-CreERS (Zhang et al., 2015) to *Rosa26*tdRFP mice (Luche et al., 2007), heterozygous C57BL/6-Il23<sup>tm1Kuch</sup> (here IL23-R-eGFP) mice (Awasthi et al., 2009), and *Tcrd*-H2BeGFP (Prinz et al., 2006) mice were bred and housed under specific pathogen-free conditions in the central animal facility at Hannover Medical School. C57BL/6-NCrI (WT) mice were purchased from Charles River Laboratories. Unless specified otherwise, mice were ana-

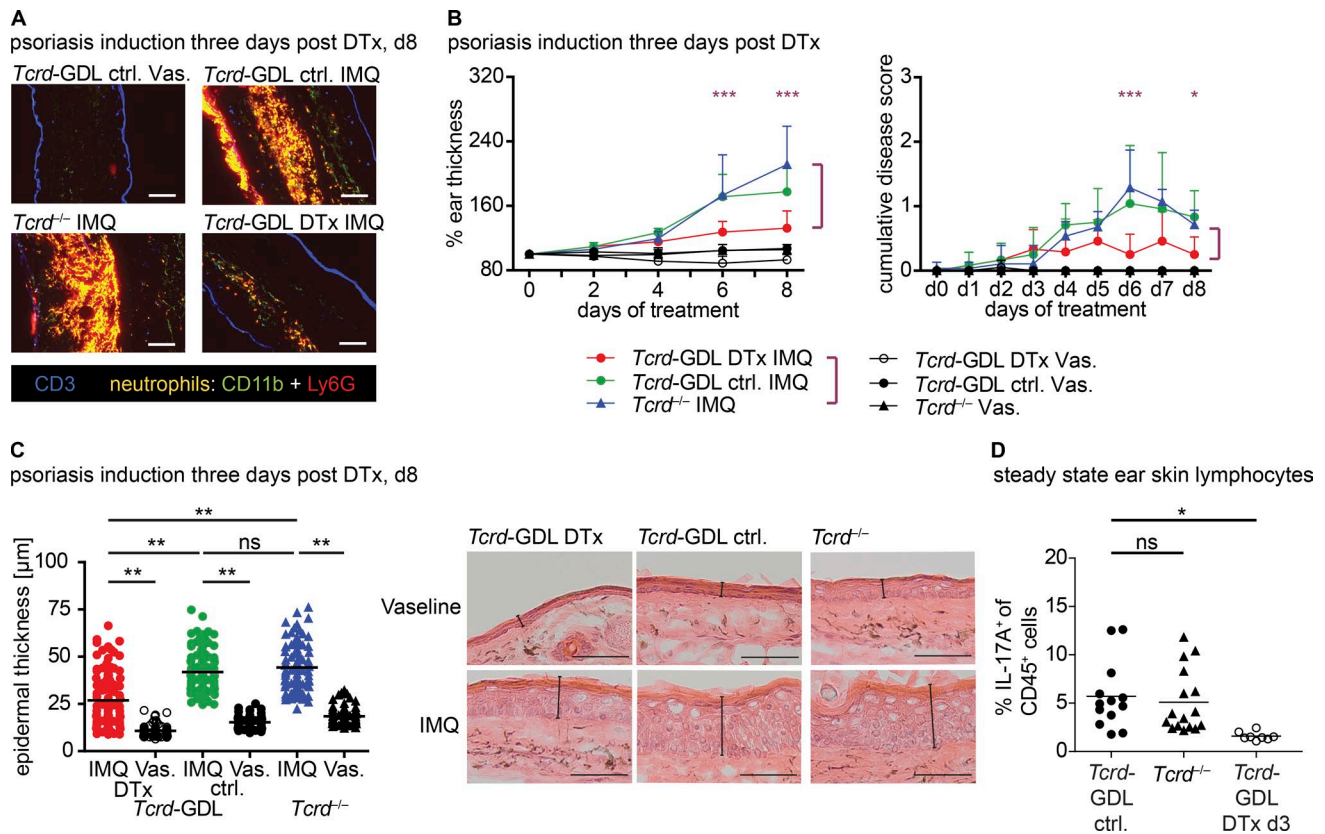


**Figure 5. Freshly  $\gamma\delta$  T cell-depleted mice develop less severe IMQ-induced psoriasis. (A–C)** IMQ-induced psoriasis. Ears of indicated genotypes were treated with IMQ or Vaseline (Vas.), starting at day 3 after  $\gamma\delta$  T cell depletion (DTx). **(A)** Ear skin immunofluorescence histology at day 8 of IMQ treatment of mice shown in B, CD3<sup>+</sup> T cells (blue), and CD11b<sup>+</sup>Ly6G<sup>+</sup> neutrophils (yellow). Bars, 100  $\mu$ m. Representative images from two independent experiments with  $n = 1$ –4 mice each. **(B)** Change of ear thickness given as percent diameter of untreated ears (day 0; left) and disease score (right) over time. Graphs show pooled data from three experiments, each one to four mice per group (total numbers of mice: seven *Tcrd*-GDL DTx IMQ; eight *Tcrd*-GDL ctrl. IMQ; seven *Tcrd*<sup>-/-</sup> IMQ; six *Tcrd*-GDL DTx Vas.; five *Tcrd*-GDL ctrl. Vas.; six *Tcrd*<sup>-/-</sup> Vas.); two-way ANOVA with Bonferroni posttests, mean  $\pm$  SD. **(C)** Epidermal hyperplasia measured on H&E-stained ear skin sections of IMQ- and Vaseline-treated ears of the indicated genotypes, respectively. Scatter plot shows quantification of the epidermal thickening measured on the sections; each dot represents one measurement acquired on 36 slides of two mice per group (left). Representative images out of two mice per group. Bars, 50  $\mu$ m (right). Data were validated in two independent experiments. **(D)** Steady state mean frequency of IL-17A-producing CD45<sup>+</sup> lymphocytes in ear skin of control (ctrl.) and  $\gamma\delta$  T cell-depleted *Tcrd*-GDL mice, day 3 (d3) after depletion, compared with *Tcrd*<sup>-/-</sup> mice by intracellular flow cytometry. Pooled data from three to five experiments with each  $n = 2$ –4 mice per group; one dot equals one mouse, mean. One-way ANOVA with Bonferroni posttests. \*,  $P < 0.05$ ; \*\*,  $P < 0.01$ ; \*\*\*,  $P < 0.001$ ; ns, not significant.

lyzed at 7–20 wk of age. All experiments were conducted according to local and institutional guidelines. The study was approved by the Lower Saxony State Office for Consumer Protection and Food Safety, file reference 33.12-42502-04-15/1889.

#### Generation of *Tcrd*-GDL mice

We inserted an expression cassette encoding eGFP, human DTR and luciferase (Luc; Suffner et al., 2010) into a modification of the vector used to generate *Tcrd*-H2BeGFP mice (Prinz et al., 2006). Electroporation and homologous recombination to the 3'UTR of the *Tcrd* constant gene in JM8A3 ES cells was screened by PCR and by Southern blot. Selected ES cell clones were expanded and subsequently injected into blastocysts to generate knock-in mice on the C57BL/6 genetic background (*Tcrd*-GDL mice). Chimerism in F0 offspring was identified by fur color, positive F0 offspring were mated with C57BL/6N mice, and F1 offspring were tested for germline transmission and successful excision of the Neo cassette by PCR (PCR primers: GDL $\delta$  forward: 5'-CTAGAAGAAAAG

CAAAAGCCCTC-3'; GDL-IRES reverse: 5'-AAACGCACACCGGCC TTATT-3'; GDL $\delta$  reverse: 5'-CCTTCCTTTTCGGTATTTTACTTTCA-3'; knock-in fragment size: 412-bp; WT fragment size: 519 bp).

#### $\gamma\delta$ T cell depletion

For conditional depletion of  $\gamma\delta$  T cells mice were treated with 30 ng DTx per gram body weight by i.p. injection. The optimal regimen for quantitative  $\gamma\delta$  T cell depletion was titrated as two injections of 15  $\mu$ g DTx per gram body weight separated by 48 h. This DTx treatment regimen did not affect lymphocytes in WT mice in control experiments. *Tcrd*-GDL mice in control groups were injected with PBS (*Tcrd*-GDL ctrl.). In experiments comparing *Tcrd*-GDL control and DTx treated mice, we used littermates.

*Tcrd*-Cre induction *Tcrd*CreER  $\times$  R26tdRFP mice were gavaged with 4 mg tamoxifen citrate (Enzo Life Sciences), dissolved in 400  $\mu$ l corn oil/ethanol, three times every other day to induce Cre expression and subsequently RFP expression by  $\gamma\delta$  T cells.

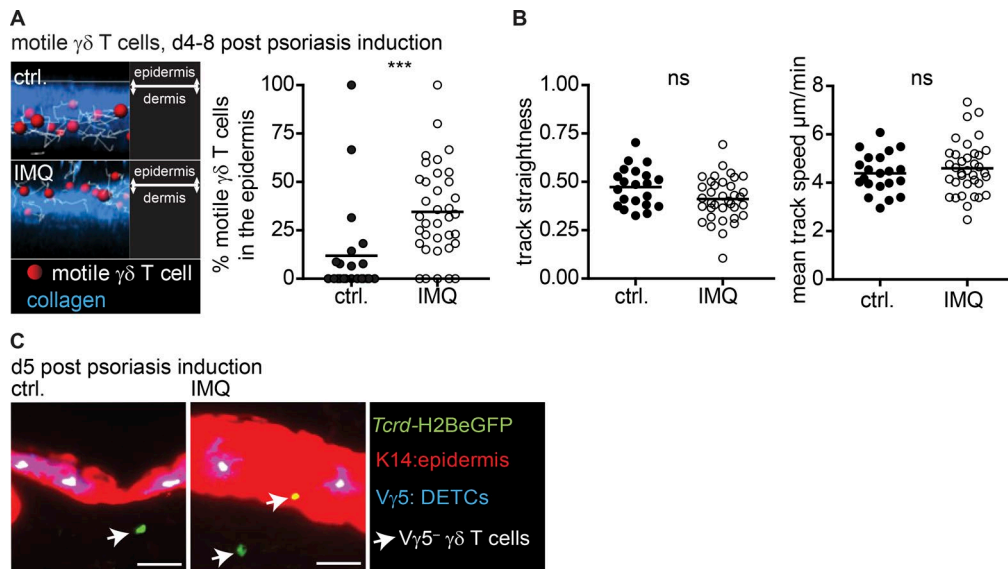


**Figure 6. Dermal  $\gamma\delta$  T cells translocate into epidermis under inflammatory conditions. (A and B)** In vivo two-photon imaging of *Tcrd*-GDL Vaseline- (ctrl.) and IMQ-treated ear skin, respectively. Shown are pooled data from three experiments with each one to two mice per group, Student's *t* test. **(A)** Using IMA RIS software motile dermal  $\gamma\delta$  T cells (red dots) were tracked and dermis was defined as surface by second harmonics signal corresponding to collagen (blue, right). Frequency of motile  $\gamma\delta$  T cells in epidermis (see Video 4), one dot per video (left). **(B)** Scatter plots show track straightness (displacement length divided by track length, left) and mean track speed (right). **(C)** Ear skin histology of inflamed *Tcrd*-H2BeGFP ears (representative image of two different stainings). Mice were treated for five consecutive days with Vaseline (ctrl.) or IMQ-containing cream (Aldara; IMQ). Red: epidermis (keratin 14); green: GFP<sup>+</sup>  $\gamma\delta$  T cells below epidermis; purple: GFP<sup>+</sup> V $\gamma$ 5<sup>+</sup> dendritic epidermal T cells (blue V $\gamma$ 5<sup>+</sup> cells); yellow: GFP<sup>+</sup>V $\gamma$ 5<sup>-</sup> dermal  $\gamma\delta$  T cells within epidermis. Bars, 50  $\mu\text{m}$ . \*, *P* < 0.05; \*\*, *P* < 0.01; \*\*\*, *P* < 0.001; ns, not significant.

### In vivo imaging system (IVIS)

IVIS 200 system (PerkinElmer) and Living Image software 2.50.2 (Caliper LifeScience) was used for detection of bioluminescence. For images shown, mice were sacrificed 10 min after i.p. injection of 400  $\mu\text{g}$  D-luciferin.

### IMQ-induced psoriasis

To induce psoriasis, both ears were treated daily with 5 mg Aldara cream (5% IMQ) per ear for seven consecutive days. Ear thickness was measured starting 2 d before the first treatment (day 0) and set to 100%. Ear thickness was measured using a caliper. Reddening and scaling were evaluated daily and scored with 0: no change, 1: mild, 2: moderate, and 3: severe. Reddening and scaling were assessed separately to calculate an average cumulative disease score. For treatment, mice were anesthetized with Ketamin/Rompun and supplemented i.p. with 0.9% NaCl to avoid dehydration.

### Preparation and staining of epidermal sheets

Fur was carefully removed from mouse ears using a scalpel and dorsal and ventral parts were separated. Subsequently, with dermal side down, they were incubated on 0.5 M NH<sub>4</sub>SCN at 37°C for 20 min. Afterward, epidermis was peeled off and fixed using 4% paraformaldehyde at room temperature for 15 min. Before antibody staining epidermal layers were rehydrated in PBS for 20 min at room temperature and blocked with 8% rat serum. Sheets were stained with the indicated antibodies for 2 h at room temperature and analyzed with an Olympus BX641 microscope. Antibodies directed against TCR $\beta$  (clone H57-597; Alexa Fluor 488) and V $\gamma$ 5 (clone 536; APC) were purchased from BioLegend. An-

ti-CD3 (clone 17A2) was produced from a rat hybridoma cell line and subsequently labeled with Cy5 or Cy3.

### Skin histology

Ear skin was frozen in Tissue Tek optimal cutting temperature compound (Sakura Finetek) and 8- $\mu\text{m}$  cryosections were cut using a cryo microtome (CM3050; Leica). Cryosections were fixed for 10 min with ice-cold acetone and stored at -20°C or used directly for staining. Slides were either stained with H&E or for immunofluorescent microscopy with the indicated antibodies. All samples were covered with Mowiol and examined with an Olympus BX641 fluorescence microscope using CellSense Dimension software (Olympus). Following antibodies were used: anti-CD3 clone 17A2 (Cy5; rat hybridoma cell line), anti-Ly6G clone 1A8 (PE; BioLegend), anti-CD11b clone MAC-1 (FITC; rat hybridoma cell line), anti-cytokeratin K14 clone Poly19053 (unlabeled; BioLegend), and anti-rabbit polyclonal (Cy3, Dianova) to detect the K14 antibody.

### Flow cytometry

Single-cell suspension from peripheral lymph nodes, spleen and liver were prepared by meshing the organs through nylon gaze or 100  $\mu\text{m}$  nylon cell strainers (Falcon), respectively. Subsequently, liver lymphocytes were purified by density gradient centrifugation using Percoll gradients. For the preparation of ear skin lymphocytes, four separated halves of one ear pair were digested with collagenase IV (2 mg/ml; Worthington) and DNase I (187.5  $\mu\text{g}/\text{ml}$ ) for 1 h 30 min at 37°C. For the last 15 min of incubation EDTA (final concentration, 37.5 mM) was added. Subsequently, remaining tissue was dissociated mechanically facilitating a 1-2-



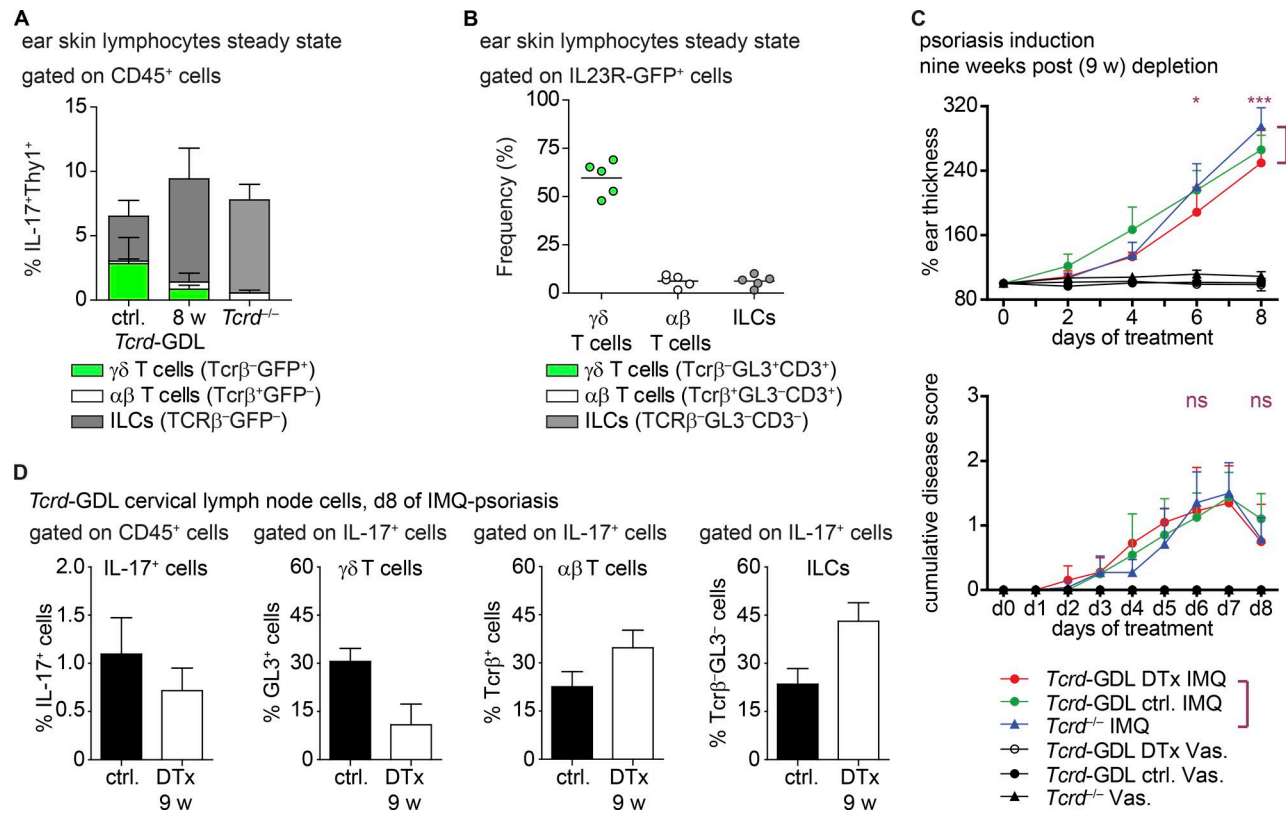


**Figure 7.  $\alpha\beta$  T cells and ILCs can compensate absent  $\gamma\delta$ 17 cells.** (A) Frequencies of indicated cell populations among IL-17A<sup>+</sup> cells. *Tcrd*-GDL ctrl.: nondepleted; *Tcrd*-GDL 8w: 8 wk after  $\gamma\delta$  T cell depletion. Shown are pooled data from two experiments with each  $n = 2-4$  mice per group, mean  $\pm$  SD. (B) Frequencies of indicated cell populations among IL23R-GFP<sup>+</sup> ear skin lymphocytes from heterozygous IL23R-GFP reporter mice. Pooled data from two experiments with each  $n = 2-3$  mice per group, mean. (C) Ear thickness and disease score over time in control and IMQ-treated groups. IMQ treatment started 9 wk after  $\gamma\delta$  T cell depletion. Graphs show pooled data from two experiments, each  $n = 1-3$  mice per group (total numbers of mice: five *Tcrd*-GDL DTx IMQ; six *Tcrd*-GDL ctrl. IMQ; six *Tcrd*<sup>-/-</sup> IMQ; two *Tcrd*-GDL DTx Vas; three *Tcrd*-GDL ctrl. Vas; three *Tcrd*<sup>-/-</sup> Vas); two-way ANOVA with Bonferroni posttests, mean  $\pm$  SD. (D) Composition of IL-17A-producing lymphocytes from psoriatic ear skin draining lymph nodes day 8 of IMQ-psoriasis, 9 wk after  $\gamma\delta$  T cell depletion. Frequencies of indicated cell populations in nondepleted *Tcrd*-GDL control (ctrl.) compared with *Tcrd*-GDL mice that were treated with DTx 9 wk before psoriasis induction (DTx 9 w). Data shown are from one representative experiment out of two independent experiments with each  $n = 2-3$  mice per group. \*,  $P < 0.05$ ; \*\*,  $P < 0.01$ ; \*\*\*,  $P < 0.001$ ; ns, not significant.

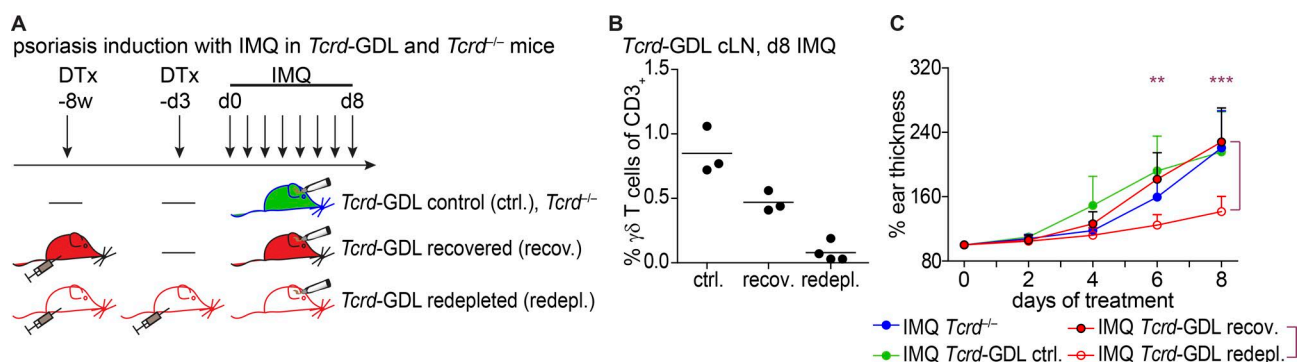


**Figure 8. Redeployment of  $\gamma\delta$  T cells confers re-protection in IMQ-induced psoriasis.** (A) For redeployment of  $\gamma\delta$  T cells, mice were treated twice with DTx at 9 wk and 3 d, before IMQ treatment. Mice of the recovered group were treated only once with DTx at 9 wk before IMQ treatment. (B) Littermates of *Tcrd*-GDL mice were treated as described in A. Mean frequency of cervical LN (cLN)  $\gamma\delta$  T cells of d8 IMQ-treated *Tcrd*-GDL mice. One dot represents one mouse; one experiment representative of two is shown. (C) Ear thickness over time of indicated groups. IMQ treatment started 9 wk after first  $\gamma\delta$  T cell depletion. Shown are pooled data from two independent experiments with each two to four mice per group, mean  $\pm$  SD. \*,  $P < 0.05$ ; \*\*,  $P < 0.01$ ; \*\*\*,  $P < 0.001$ ; ns, not significant.

cm long 19-G syringe needle and filtered through 50  $\mu$ m CellTrics (Sysmex). Afterward, lymphocytes were isolated by density gradient centrifugation using Percoll gradients.

Before antibody staining, Fc-receptors were blocked with FcR antibody (clone 2.4G2) on ice for 5 min. For intracellular staining, BD Biosciences Cytofix/Cytoperm Fixation/Permeabilization kit was used according to the manufacturer's instructions. Live/dead discrimination in intracellular cytokine staining protocols was performed using Zombi Aqua Fixable Viability kit (BioLegend; A.dead) according to manufacturer's instructions. Antibodies directed against CD3 (clone 17A2; APCVio770), TCR $\beta$  (clone REA318; APCVio770), CD45.2 (clone 104-2; PerCPVio700 or VioGreen), and CD44 (clone IM7.8.1; VioBlue) were purchased from Miltenyi Biotec. Antibodies directed against CD3 (clone 145-2C11; PECy7) and IL-17A (clone eBio17B7; Alexa647) were from eBioscience. The following antibodies were produced from rat hybridoma cell lines and subsequently labeled with the indicated fluorochromes: anti-CD3 clone 17A2 (Cy5), anti-CD4 clone RMCD4-2 (Cy 5), anti-CD8 $\beta$  clone RMCD8-2 (Pacific Orange), anti-TCR $\gamma\delta$  clone GL3 (Alexa488), and anti-V $\gamma$ 4 clone 49.2 (subclone 49.2-9, Cy5). Antibodies directed against V $\gamma$ 5 (clone 536, APC), CD27 (clone LG.7F9, PerCPy5.5), V $\gamma$ 1 (clone 2.11, PE), NK1.1 (clone PK136, PECy7), IL-17A (clone TC1118H10.1, PE), and CD19 (clone 6D5, PECy7) were purchased from BioLegend. Staining of V $\gamma$ 6 was performed as described previously (Roark et al., 2004). In short, the IgM anti-V $\gamma$ 5 clone 17D1 binds additionally to TCRs using the V $\gamma$ 6 chain after preincubation of cells with anti-TCR $\gamma\delta$  (clone GL3). Subsequently, 17D1 was detected with anti-IgM PE (clone RM-7B4; eBioscience).

### Two-photon laser-scanning in vivo imaging

An upright Leica DM LFSA microscope equipped with a 20  $\times$  0.95 numerical aperture water immersion objective (Olympus) and a pulsed Ti:Sa infrared laser (MaiTai, Spectra Physics) turned to 920 nm was used for two-photon laser-scanning microscopy. During image acquisition, ears were fixed with a coverslip on a custom build metal plate heated to 37°C. For detection of eGFP nondescanned, detectors fitted with 525/50 band pass filter were facilitated; for detection of second harmonics and Hoechst 33342, 447/60 band pass filters were used. Hoechst 33342 was used to visualize nuclei during small intestine in vivo imaging. During ear skin imaging the second harmonics signal was used to identify collagen-rich tissues like the dermis. Longitudinal imaging of skin  $\gamma\delta$  T cell recovery was applied to the same mice at indicated time points after  $\gamma\delta$  T cell depletion. Control mice were injected with PBS (control).

For localization of motile  $\gamma\delta$  T cells in inflamed skin, ears of *Tcrd*-GDL or *Tcrd*-H2BeGFP mice were treated for four to seven consecutive days with Vaseline (control) or IMQ Using IMARIS 7.6.4 software (Bitplane); motile GFP $^{+}$   $\gamma\delta$  T cells were defined with red dots and tracked. The surface of dermis was visualized by surface rendering of the second harmonics signal of the collagen localized in the dermis.

### High-throughput TCR sequencing

For mRNA-based TCR analysis, paired-end Illumina sequencing was performed as described (Ravens et al., 2017). In brief, for

mRNA isolation sorted CD44<sup>high</sup>Ly6C<sup>+</sup>V $\gamma$ 4<sup>+</sup> peripheral lymph node cells were pooled from seven to eight *Tcrd*-GDL control- and DTx-treated mice each (RNase mini kit; Qiagen). Subsequently, mRNA was reverse transcribed into cDNA (superscript III; Invitrogen). CDR3 regions of *Tcr $\gamma$*  and *Tcr $\delta$*  were PCR-amplified using Taq polymerase (Invitrogen) and gene-specific primers targeting TCR variable (V)- and constant (C)-regions with Illumina sequencing adapter sequences as overhangs (5'-GTCTCGTGGGCTCGGAGA TGTGTATAAGAGACAG and TCGTCGGCAGCGTCAGATGTGTAT AAGAGACAG-3'). Gene-specific primer sequences were for TrgV4: 5'-TCCTTGGAGGAAGAAGACGA-3'; TrgC: 5'-CTTATGGAGATTGT TTCAGCA-3'; TrdV5: 5'-TAGGGACGACACTAGTTCCCATGAT-3'; TrdC: 5'-ATGATGAAAACAGATGGTTTGG-3'. Each PCR reaction contained 5–7.5  $\mu$ l cDNA as template in a final volume of 20  $\mu$ l. PCR products were size selected on 1% agarose gels and purified with Qiagen gel extraction kits. For paired-end 500-cycle Illumina Mi-Seq analysis, amplicons were coded with Nextera Index primers. Sequencing libraries were calibrated to 4 nM and processed according to the Illumina "denature and dilution guide." 20% PhIX was added to control sequencing performance and for warranting library diversity. Generated Fastq files were annotated according to IMG/High-Vquest (Alamyar et al., 2012). For downstream analysis, only productive sequences with unambiguous V-gene segment were considered. *Tcr $\gamma$*  and *Tcr $\delta$*  clonotypes were identified based on identical CDR3 region sequences. Results are presented as percentages of all productive reads per sample to normalize between samples. All R and bash shell scripts were based on previous analysis strategies (Ravens et al., 2017). TCR sequences are published under SRA number SRP130082.

### Statistical analyses

All statistical analyses were performed using GraphPad Prism software (Version 4.03). Differences between individual groups were analyzed for statistical significance as indicated in legends using either unpaired Student's *t* test, one-way, or two-way ANOVA followed by Dunn's Multiple Comparison or Bonferroni posttests. *P* values < 0.05 were considered as significant different (\*, *P* < 0.05; \*\*, *P* < 0.01; \*\*\*, *P* < 0.001).

### Online supplemental material

Fig. S1 illustrates the strategy used to generate *Tcrd*-GDL mice. Fig. S2 shows further characterization of *Tcrd*-GDL mice including depletion efficiency. Fig. S3 shows differential recovery of  $\gamma\delta$  T cell populations after depletion. Fig. S4 focuses on the empty DETC niche after depletion. Further supplemental material includes four in vivo two-photon imaging videos. Videos 1 and 2 show  $\gamma\delta$  T cell motility in ear skin and small intestine, respectively. Video 3 shows recovery of skin  $\gamma\delta$  T cells over time. Video 4 compares  $\gamma\delta$  T cells in healthy and psoriatic inflamed ear skin.

### Acknowledgments

We would like to acknowledge the assistance of the Cell Sorting Core Facility of the Hannover Medical School. Further, we thank Pablo Pereira for providing anti-V $\gamma$ 4 clone 49.2 (Department of Immunology, Pasteur Institut, Paris, France).

The work was supported by grants from the Deutsche Forschungsgemeinschaft (PR727/8-1 and SFB900-B8 to I. Prinz) and from Hannover Biomedical Research School (HBRS/DEW IN to I. Sandrock).

The authors declare no competing financial interests.

Author contributions: I. Sandrock, A. Reinhardt, and S. Ravens designed and performed experiments and discussed and analyzed data; C. Binz, A. Wilharm, J. Martins, L. Oberdörfer, L. Tan, S. Lienenklaus, and R. Nauman helped with performing experiments and data analysis; B. Zhang, Y. Zhuang, A. Krueger, and R. Förster helped supervise research and discussed data; I. Prinz supervised research and discussed and analyzed data; and I. Sandrock and I. Prinz wrote the manuscript.

Submitted: 30 July 2018

Revised: 14 September 2018

Accepted: 23 October 2018

## References

- Alamyar, E., P. Duroux, M.P. Lefranc, and V. Giudicelli. 2012. IMGT<sup>®</sup> tools for the nucleotide analysis of immunoglobulin (IG) and T cell receptor (TR) V-(D)-J repertoires, polymorphisms, and IG mutations: IMGT/V-QUEST and IMGT/HighV-QUEST for NGS. *Methods Mol. Biol.* 882:569–604.
- Audemard-Verger, A., M. Rivière, A. Durand, E. Peranzoni, V. Guichard, P. Hamon, N. Bonilla, T. Guilbert, A. Boissonnas, C. Auffray, et al. 2017. Macrophages Induce Long-Term Trapping of  $\gamma\delta$  T Cells with Innate-like Properties within Secondary Lymphoid Organs in the Steady State. *J. Immunol.* 199:1998–2007.
- Awasthi, A., L. Riolo-Blanco, A. Jäger, T. Korn, C. Pot, G. Galileos, E. Bettelli, V.K. Kuchroo, and M. Oukka. 2009. Cutting edge: IL-23 receptor gfp reporter mice reveal distinct populations of IL-17-producing cells. *J. Immunol.* 182:5904–5908.
- Blink, S.E., M.W. Caldis, G.E. Goings, C.T. Harp, B. Malissen, I. Prinz, D. Xu, and S.D. Miller. 2014.  $\gamma\delta$  T cell subsets play opposing roles in regulating experimental autoimmune encephalomyelitis. *Cell. Immunol.* 290:39–51.
- Cai, Y., X. Shen, C. Ding, C. Qi, K. Li, X. Li, V.R. Jala, H.G. Zhang, T. Wang, J. Zheng, and J. Yan. 2011. Pivotal role of dermal IL-17-producing  $\gamma\delta$  T cells in skin inflammation. *Immunity*. 35:596–610.
- Carabana, J., E. Ortigoza, and M.S. Krangel. 2005. Regulation of the murine Ddelta2 promoter by upstream stimulatory factor 1, Runx1, and c-Myb. *J. Immunol.* 174:4144–4152.
- Chennupati, V., T. Worbs, X. Liu, F.H. Malinarich, S. Schmitz, J.D. Haas, B. Malissen, R. Förster, and I. Prinz. 2010. Intra- and intercompartmental movement of gammadelta T cells: intestinal intraepithelial and peripheral gammadelta T cells represent exclusive nonoverlapping populations with distinct migration characteristics. *J. Immunol.* 185:5160–5168.
- Chien, Y.H., C. Meyer, and M. Bonneville. 2014.  $\gamma\delta$  T cells: first line of defense and beyond. *Annu. Rev. Immunol.* 32:121–155.
- Cho, J.S., E.M. Pietras, N.C. Garcia, R.I. Ramos, D.M. Farzam, H.R. Monroe, J.E. Magorien, A. Blauvelt, J.K. Kolls, A.L. Cheung, et al. 2010. IL-17 is essential for host defense against cutaneous *Staphylococcus aureus* infection in mice. *J. Clin. Invest.* 120:1762–1773.
- Conti, H.R., A.C. Peterson, L. Brane, A.R. Huppler, N. Hernández-Santos, N. Whibley, A.V. Garg, M.R. Simpson-Abelson, G.A. Gibson, A.J. Mamo, et al. 2014. Oral-resident natural Th17 cells and  $\gamma\delta$  T cells control opportunistic *Candida albicans* infections. *J. Exp. Med.* 211:2075–2084.
- Cua, D.J., and C.M. Tato. 2010. Innate IL-17-producing cells: the sentinels of the immune system. *Nat. Rev. Immunol.* 10:479–489.
- Di Meglio, P., F. Villanova, A.A. Navarini, A. Mylonas, I. Tosi, F.O. Nestle, and C. Conrad. 2016. Targeting CD8(+) T cells prevents psoriasis development. *J. Allergy Clin. Immunol.* 138:274–276.e6.
- Föhse, L., A. Reinhardt, L. Oberdörfer, S. Schmitz, R. Förster, B. Malissen, and I. Prinz. 2013. Differential postselection proliferation dynamics of  $\alpha\beta$  T cells, Foxp3+ regulatory T cells, and invariant NKT cells monitored by genetic pulse labeling. *J. Immunol.* 191:2384–2392.
- Gasteiger, G., X. Fan, S. Dikiy, S.Y. Lee, and A.Y. Rudensky. 2015. Tissue residency of innate lymphoid cells in lymphoid and nonlymphoid organs. *Science*. 350:981–985.
- Gladiator, A., N. Wangler, K. Trautwein-Weidner, and S. Leibundgut-Landmann. 2013. Cutting edge: IL-17-secreting innate lymphoid cells are essential for host defense against fungal infection. *J. Immunol.* 190:521–525.
- Goodman, T., and L. Lefrançois. 1989. Intraepithelial lymphocytes. Anatomical site, not T cell receptor form, dictates phenotype and function. *J. Exp. Med.* 170:1569–1581.
- Gray, E.E., K. Suzuki, and J.G. Cyster. 2011. Cutting edge: Identification of a motile IL-17-producing gammadelta T cell population in the dermis. *J. Immunol.* 186:6091–6095.
- Haas, J.D., F.H. González, S. Schmitz, V. Chennupati, L. Föhse, E. Kremmer, R. Förster, and I. Prinz. 2009. CCR6 and NK1.1 distinguish between IL-17A and IFN-gamma-producing gammadelta effector T cells. *Eur. J. Immunol.* 39:3488–3497.
- Haas, J.D., S. Ravens, S. Düber, I. Sandrock, L. Oberdörfer, E. Kashani, V. Chennupati, L. Föhse, R. Naumann, S. Weiss, et al. 2012. Development of interleukin-17-producing  $\gamma\delta$  T cells is restricted to a functional embryonic wave. *Immunity*. 37:48–59.
- Hammar, H., S.Q. Gu, A. Johannesson, K.G. Sundkvist, and P. Biberfeld. 1984. Subpopulations of mononuclear cells in microscopic lesions of psoriatic patients. Selective accumulation of suppressor/cytotoxic T cells in epidermis during the evolution of the lesion. *J. Invest. Dermatol.* 83:416–420.
- Hartwig, T., S. Pantelyushin, A.L. Croxford, P. Kulig, and B. Becher. 2015. Dermal IL-17-producing  $\gamma\delta$  T cells establish long-lived memory in the skin. *Eur. J. Immunol.* 45:3022–3033.
- Houlden, B.A., L.A. Matis, R.Q. Cron, S.M. Widacki, G.D. Brown, C. Pampeno, D. Meruelo, and J.A. Bluestone. 1989. A TCR gamma delta cell recognizing a novel TL-encoded gene product. *Cold Spring Harb. Symp. Quant. Biol.* 54:45–55.
- Huang, Y., R.A. Heiser, T.O. Detanico, A. Getahun, G.A. Kirchenbaum, T.L. Casper, M.K. Aydintug, S.R. Carding, K. Ikuta, H. Huang, et al. 2015.  $\gamma\delta$  T cells affect IL-4 production and B-cell tolerance. *Proc. Natl. Acad. Sci. USA*. 112:E39–E48.
- Huang, Y., A. Getahun, R.A. Heiser, T.O. Detanico, K. Aviszus, G.A. Kirchenbaum, T.L. Casper, C. Huang, M.K. Aydintug, S.R. Carding, et al. 2016.  $\gamma\delta$  T Cells Shape Preimmune Peripheral B Cell Populations. *J. Immunol.* 196:217–231.
- Itoharu, S., P. Mombaerts, J. Lafaille, J. Iacomini, A. Nelson, A.R. Clarke, M.L. Hooper, A. Farr, and S. Tonegawa. 1993. T cell receptor delta gene mutant mice: independent generation of alpha beta T cells and programmed rearrangements of gamma delta TCR genes. *Cell*. 72:337–348.
- Jameson, J.M., G. Cauvi, D.A. Witherden, and W.L. Havran. 2004. A keratinocyte-responsive gamma delta TCR is necessary for dendritic epidermal T cell activation by damaged keratinocytes and maintenance in the epidermis. *J. Immunol.* 172:3573–3579.
- Jensen, K.D., X. Su, S. Shin, L. Li, S. Youssef, S. Yamasaki, L. Steinman, T. Saito, R.M. Locksley, M.M. Davis, et al. 2008. Thymic selection determines gammadelta T cell effector fate: antigen-naïve cells make interleukin-17 and antigen-experienced cells make interferon gamma. *Immunity*. 29:90–100.
- Jiang, X., C.O. Park, J. Geddes Sweeney, M.J. Yoo, O. Gaide, and T.S. Kupper. 2017. Dermal  $\gamma\delta$  T Cells Do Not Freely Re-Circulate Out of Skin and Produce IL-17 to Promote Neutrophil Infiltration during Primary Contact Hypersensitivity. *PLoS One*. 12:e0169397.
- Kashani, E., L. Föhse, S. Raha, I. Sandrock, L. Oberdörfer, C. Koenecke, S. Suherbaum, S. Weiss, and I. Prinz. 2015. A clonotypic V $\gamma$ 4J $\gamma$ 1/V $\delta$ 5D $\delta$ 2J $\delta$ 1 innate  $\gamma\delta$  T-cell population restricted to the CCR6<sup>+</sup>CD27<sup>+</sup> subset. *Nat. Commun.* 6:6477.
- Kaufmann, S.H., C. Blum, and S. Yamamoto. 1993. Crosstalk between alpha/beta T cells and gamma/delta T cells in vivo: activation of alpha/beta T-cell responses after gamma/delta T-cell modulation with the monoclonal antibody GL3. *Proc. Natl. Acad. Sci. USA*. 90:9620–9624.
- Ke, Y., K. Pearce, J.P. Lake, H.K. Ziegler, and J.A. Kapp. 1997. Gamma delta T lymphocytes regulate the induction and maintenance of oral tolerance. *J. Immunol.* 158:3610–3618.
- Koenecke, C., V. Chennupati, S. Schmitz, B. Malissen, R. Förster, and I. Prinz. 2009. In vivo application of mAb directed against the gammadelta TCR does not deplete but generates “invisible” gammadelta T cells. *Eur. J. Immunol.* 39:372–379.
- Kohlgruber, A.C., S.T. Gal-Oz, N.M. LaMarche, M. Shimazaki, D. Duquette, H.N. Nguyen, A.I. Mina, T. Paras, A. Tavakkoli, U. von Andrian, et al. 2018.  $\gamma\delta$  T cells producing interleukin-17A regulate adipose regulatory T cell homeostasis and thermogenesis. *Nat. Immunol.* 19:464–474.



- Koo, G.C., and J.R. Peppard. 1984. Establishment of monoclonal anti-Nk-1.1 antibody. *Hybridoma*. 3:301–303.
- Korn, T., and F. Petermann. 2012. Development and function of interleukin 17-producing  $\gamma\delta$  T cells. *Ann. N. Y. Acad. Sci.* 1247:34–45.
- Laggner, U., P. Di Meglio, G.K. Perera, C. Hundhausen, K.E. Lacy, N. Ali, C.H. Smith, A.C. Hayday, B.J. Nickoloff, and F.O. Nestle. 2011. Identification of a novel proinflammatory human skin-homing V $\gamma$ 9V $\delta$ 2 T cell subset with a potential role in psoriasis. *J. Immunol.* 187:2783–2793.
- Lahl, K., and T. Sparwasser. 2011. In vivo depletion of FoxP3+ Tregs using the DERE mouse model. *Methods Mol. Biol.* 707:157–172.
- Lucche, H., O. Weber, T. Nageswara Rao, C. Blum, and H.J. Fehling. 2007. Faithful activation of an extra-bright red fluorescent protein in “knock-in” Cre-reporter mice ideally suited for lineage tracing studies. *Eur. J. Immunol.* 37:43–53.
- Mabuchi, T., T. Takekoshi, and S.T. Hwang. 2011. Epidermal CCR6+  $\gamma\delta$  T cells are major producers of IL-22 and IL-17 in a murine model of psoriasisiform dermatitis. *J. Immunol.* 187:5026–5031.
- Mabuchi, T., T.P. Singh, T. Takekoshi, G.F. Jia, X. Wu, M.C. Kao, I. Weiss, J.M. Farber, and S.T. Hwang. 2013. CCR6 is required for epidermal trafficking of  $\gamma\delta$ -T cells in an IL-23-induced model of psoriasisiform dermatitis. *J. Invest. Dermatol.* 133:164–171.
- Mamedov, M.R., A. Scholzen, R.V. Nair, K. Cumnock, J.A. Kenkel, J.H.M. Oliveira, D.L. Trujillo, N. Saligrama, Y. Zhang, F. Rubelt, et al. 2018. A Macrophage Colony-Stimulating-Factor-Producing  $\gamma\delta$  T Cell Subset Prevents Malarial Parasitemic Recurrence. *Immunity*. 48:350–363.e7.
- Matos, T.R., J.T. O'Malley, E.L. Lowry, D. Hamm, I.R. Kirsch, H.S. Robins, T.S. Kupper, J.G. Krueger, and R.A. Clark. 2017. Clinically resolved psoriatic lesions contain psoriasis-specific IL-17-producing  $\alpha\beta$  T cell clones. *J. Clin. Invest.* 127:4031–4041.
- McCaughy, T.M., M.S. Wilken, and K.A. Hogquist. 2007. Thymic emigration revisited. *J. Exp. Med.* 204:2513–2520.
- Merleev, A.A., A.I. Marusina, C. Ma, J.T. Elder, L.C. Tsoi, S.P. Raychaudhuri, S. Weidinger, E.A. Wang, I.E. Adamopoulos, G. Luxardi, et al. 2018. Meta-analysis of RNA sequencing datasets reveals an association between TRAJ23, psoriasis, and IL-17A. *JCI Insight*. 3:e120682.
- Misiak, A., M.M. Wilk, M. Raverdeau, and K.H. Mills. 2017. IL-17-Producing Innate and Pathogen-Specific Tissue Resident Memory  $\gamma\delta$  T Cells Expand in the Lungs of Bordetella pertussis-Infected Mice. *J. Immunol.* 198:363–374.
- Mombaerts, P., J. Arnoldi, F. Russ, S. Tonegawa, and S.H. Kaufmann. 1993. Different roles of alpha beta and gamma delta T cells in immunity against an intracellular bacterial pathogen. *Nature*. 365:53–56.
- Muschawek, A., V.R. Buchholz, A. Fellenzer, C. Hessel, P.A. König, S. Tao, R. Tao, M. Heikenwälder, D.H. Busch, T. Korn, et al. 2016. Antigen-dependent competition shapes the local repertoire of tissue-resident memory CD8+ T cells. *J. Exp. Med.* 213:3075–3086.
- Muschawek, A., F. Petermann, and T. Korn. 2017. IL-1 $\beta$  and IL-23 Promote Extrathymic Commitment of CD27<sup>+</sup>CD122<sup>+</sup>  $\gamma\delta$  T Cells to  $\gamma\delta$ T17 Cells. *J. Immunol.* 199:2668–2679.
- Naik, S., N. Bouladoux, J.L. Linehan, S.J. Han, O.J. Harrison, C. Wilhelm, S. Conlan, S. Himmelfarb, A.L. Byrd, C. Deming, et al. 2015. Commensal-dendritic-cell interaction specifies a unique protective skin immune signature. *Nature*. 520:104–108.
- Pantelyushin, S., S. Haak, B. Ingold, P. Kulig, F.L. Heppner, A.A. Navarini, and B. Becher. 2012. Ror $\gamma$ t+ innate lymphocytes and  $\gamma\delta$  T cells initiate psoriasisiform plaque formation in mice. *J. Clin. Invest.* 122:2252–2256.
- Papotto, P.H., N. Gonçalves-Sousa, N. Schmolka, A. Iseppon, S. Mensurado, B. Stockinger, J.C. Ribot, and B. Silva-Santos. 2017a. IL-23 drives differentiation of peripheral  $\gamma\delta$ 17 T cells from adult bone marrow-derived precursors. *EMBO Rep.* 18:1957–1967.
- Papotto, P.H., J.C. Ribot, and B. Silva-Santos. 2017b. IL-17<sup>+</sup>  $\gamma\delta$  T cells as kick-starters of inflammation. *Nat. Immunol.* 18:604–611.
- Papotto, P.H., A. Reinhardt, I. Prinz, and B. Silva-Santos. 2018. Innately versatile:  $\gamma\delta$ 17 T cells in inflammatory and autoimmune diseases. *J. Autoimmun.* 87:26–37.
- Payer, E., A. Elbe, and G. Stingl. 1991. Circulating CD3<sup>+</sup>/T cell receptor V gamma 3+ fetal murine thymocytes home to the skin and give rise to proliferating dendritic epidermal T cells. *J. Immunol.* 146:2536–2543.
- Petermann, F., V. Rothhammer, M.C. Claussen, J.D. Haas, L.R. Blanco, S. Heink, I. Prinz, B. Hemmer, V.K. Kuchroo, M. Oukka, and T. Korn. 2010.  $\gamma\delta$  T cells enhance autoimmunity by restraining regulatory T cell responses via an interleukin-23-dependent mechanism. *Immunity*. 33:351–363.
- Pöllinger, B., T. Junt, B. Metzler, U.A. Walker, A. Tyndall, C. Allard, S. Bay, R. Keller, F. Raulf, F. Di Padova, et al. 2011. Th17 cells, not IL-17+  $\gamma\delta$  T cells, drive arthritic bone destruction in mice and humans. *J. Immunol.* 186:2602–2612.
- Prinz, I., A. Sansoni, A. Kissenpfennig, L. Ardouin, M. Malissen, and B. Malissen. 2006. Visualization of the earliest steps of gammadelta T cell development in the adult thymus. *Nat. Immunol.* 7:995–1003.
- Prinz, I., B. Silva-Santos, and D.J. Pennington. 2013. Functional development of  $\gamma\delta$  T cells. *Eur. J. Immunol.* 43:1988–1994.
- Puel, A., S. Cypowyj, J. Bustamante, J.F. Wright, L. Liu, H.K. Lim, M. Migaud, L. Israel, M. Chrabieh, M. Audry, et al. 2011. Chronic mucocutaneous candidiasis in humans with inborn errors of interleukin-17 immunity. *Science*. 332:65–68.
- Ramírez-Valle, F., E.E. Gray, and J.G. Cyster. 2015. Inflammation induces dermal V $\gamma$ 4+  $\gamma\delta$ T17 memory-like cells that travel to distant skin and accelerate secondary IL-17-driven responses. *Proc. Natl. Acad. Sci. USA*. 112:8046–8051.
- Ramsburg, E., R. Tigelaar, J. Craft, and A. Hayday. 2003. Age-dependent requirement for gammadelta T cells in the primary but not secondary protective immune response against an intestinal parasite. *J. Exp. Med.* 198:1403–1414.
- Ravens, S., C. Schultze-Florey, S. Raha, I. Sandrock, M. Drenker, L. Oberdörfer, A. Reinhardt, I. Ravens, M. Beck, R. Geffers, et al. 2017. Human  $\gamma\delta$  T cells are quickly reconstituted after stem-cell transplantation and show adaptive clonal expansion in response to viral infection. *Nat. Immunol.* 18:393–401.
- Reinhardt, A., T. Wevs, T. Worbs, S. Lienenklaus, I. Sandrock, L. Oberdörfer, T. Korn, S. Yeiss, R. Förster, and I. Prinz. 2016. Interleukin-23-Dependent  $\gamma\delta$  T Cells Produce Interleukin-17 and Accumulate in the Enthesis, Aortic Valve, and Ciliary Body in Mice. *Arthritis Rheumatol.* 68:2476–2486.
- Ribot, J.C., A. deBarros, D.J. Pang, J.F. Neves, V. Peperzak, S.J. Roberts, M. Girardi, J. Borst, A.C. Hayday, D.J. Pennington, and B. Silva-Santos. 2009. CD27 is a thymic determinant of the balance between interferon-gamma- and interleukin 17-producing gammadelta T cell subsets. *Nat. Immunol.* 10:427–436.
- Roark, C.L., M.K. Aydintug, J. Lewis, X. Yin, M. Lahn, Y.S. Hahn, W.K. Born, R.E. Tigelaar, and R.L. O'Brien. 2004. Subset-specific, uniform activation among V gamma 6/V delta 1+ gamma delta T cells elicited by inflammation. *J. Leukoc. Biol.* 75:68–75.
- Roberts, S.J., A.L. Smith, A.B. West, L. Wen, R.C. Findly, M.J. Owen, and A.C. Hayday. 1996. T-cell alpha beta + and gamma delta + deficient mice display abnormal but distinct phenotypes toward a natural, widespread infection of the intestinal epithelium. *Proc. Natl. Acad. Sci. USA*. 93:11774–11779.
- Romagnoli, P.A., B.S. Sheridan, Q.M. Pham, L. Lefrançois, and K.M. Khanna. 2016. IL-17A-producing resident memory  $\gamma\delta$  T cells orchestrate the innate immune response to secondary oral *Listeria monocytogenes* infection. *Proc. Natl. Acad. Sci. USA*. 113:8502–8507.
- Rose, M.E., P. Hesketh, L. Rothwell, and R.A. Gramzinski. 1996. T-cell receptor gamma--delta lymphocytes and *Eimeria vermiformis* infection. *Infect. Immun.* 64:4854–4858.
- Stockenhuber, K., A.N. Hegazy, N.R. West, N.E. Ilott, A. Stockenhuber, S.J. Bullers, E.E. Thornton, I.C. Arnold, A. Tucci, H. Waldmann, et al. 2018. Foxp3<sup>+</sup> T reg cells control psoriasisiform inflammation by restraining an IFN- $\gamma$ -driven CD8<sup>+</sup> T cell response. *J. Exp. Med.* 215:1987–1998.
- Suffner, J., K. Hochweller, M.C. Kühnle, X. Li, R.A. Kroczeck, N. Garbi, and G.J. Hämmerling. 2010. Dendritic cells support homeostatic expansion of Foxp3+ regulatory T cells in Foxp3<sup>+</sup>LuciDTR mice. *J. Immunol.* 184:1810–1820.
- Sumaria, N., B. Roediger, L.G. Ng, J. Qin, R. Pinto, L.L. Cavanagh, E. Shklovskaya, B. Fazekas de St Groth, J.A. Triccas, and W. Weninger. 2011. Cutaneous immunosurveillance by self-renewing dermal gammadelta T cells. *J. Exp. Med.* 208:505–518.
- Sutton, C.E., L.A. Mielke, and K.H. Mills. 2012. IL-17-producing  $\gamma\delta$  T cells and innate lymphoid cells. *Eur. J. Immunol.* 42:2221–2231.
- Ugur, M., A. Kaminski, and O. Pabst. 2018. Lymph node  $\gamma\delta$  and  $\alpha\beta$  CD8<sup>+</sup> T cells share migratory properties. *Sci. Rep.* 8:8986.
- van Blijswijk, J., B.U. Schraml, and C. Reis e Sousa. 2013. Advantages and limitations of mouse models to deplete dendritic cells. *Eur. J. Immunol.* 43:22–26.
- van der Fits, L., S. Mourits, J.S. Voerman, M. Kant, L. Boon, J.D. Laman, F. Cornelissen, A.M. Mus, E. Florença, E.P. Prens, and E. Lubberts. 2009. Imiquimod-induced psoriasis-like skin inflammation in mice is mediated via the IL-23/IL-17 axis. *J. Immunol.* 182:5836–5845.
- Voehringer, D., H.E. Liang, and R.M. Locksley. 2008. Homeostasis and effector function of lymphopenia-induced “memory-like” T cells in constitutively T cell-depleted mice. *J. Immunol.* 180:4742–4753.

- Walzer, T., M. Bléry, J. Chaix, N. Fuseri, L. Chasson, S.H. Robbins, S. Jaeger, P. André, L. Gauthier, L. Daniel, et al. 2007. Identification, activation, and selective in vivo ablation of mouse NK cells via NKp46. *Proc. Natl. Acad. Sci. USA*. 104:3384–3389.
- Wei, Y.L., A. Han, J. Glanville, F. Fang, L.A. Zuniga, J.S. Lee, D.J. Cua, and Y.H. Chien. 2015. A Highly Focused Antigen Receptor Repertoire Characterizes  $\gamma\delta$  T Cells That are Poised to Make IL-17 Rapidly in Naive Animals. *Front. Immunol.* 6:118.
- Welniak, L.A., A.R. Khaled, M.R. Anver, K.L. Komschlies, R.H. Wilttrout, S. Durum, F.R. Ruscetti, B.R. Blazar, and W.J. Murphy. 2001. Gastrointestinal cells of IL-7 receptor null mice exhibit increased sensitivity to irradiation. *J. Immunol.* 166:2924–2928.
- Zarin, P., T.S.H. In, E.L.Y. Chen, J. Singh, G.W. Wong, M. Mohtashami, D.L. Wiest, M.K. Anderson, and J.C. Zúñiga-Pflücker. 2018. Integration of T-cell receptor, Notch and cytokine signals programs mouse  $\gamma\delta$  T-cell effector differentiation. *Immunol. Cell Biol.* 96:994–1007.
- Zeng, X., Y.L. Wei, J. Huang, E.W. Newell, H. Yu, B.A. Kidd, M.S. Kuhns, R.W. Waters, M.M. Davis, C.T. Weaver, and Y.H. Chien. 2012.  $\gamma\delta$  T cells recognize a microbial encoded B cell antigen to initiate a rapid antigen-specific interleukin-17 response. *Immunity*. 37:524–534.
- Zhang, B., J. Wu, Y. Jiao, C. Bock, M. Dai, B. Chen, N. Chao, W. Zhang, and Y. Zhuang. 2015. Differential Requirements of TCR Signaling in Homeostatic Maintenance and Function of Dendritic Epidermal T Cells. *J. Immunol.* 195:4282–4291.